JOURNAL OF MATERIALS SCIENCE 20 (1985) 2735–2749

# Crack-tip energy absorption processes in fibre composites

J. K. WELLS*, P. W. R. BEAUMONT
*Cambridge University Engineering Department, Trumpington Street, Cambridge, UK*

Energy-absorbing processes which operate at the tip of a crack in lamina within a composite are investigated. Previous models are reviewed and revised to take account of new analyses of debonding and pull-out processes. The toughness of the lamina is then predicted using the new models and compared with the properties of the fibre, matrix and interface. Results are presented in the form of a fracture map which clearly shows the effect of constituent material properties on the lamina toughness. A parametric study identifies important variables which affect the toughness, impact performance, and notch sensitivity of laminates.

## 1. Introduction

In a previous paper [1] we describe models of debonding and pull-out around the tip of a notch in fibre composites. It was shown that both individual fibres and groups of fibres or fibre bundles, bonded by resin, could debond and pull out under monotonic loading. Expressions were presented which allow these lengths to be estimated.

This paper discusses the processes of energy absorption around the tip of a notch in a single composite ply. The absorption of energy is quantified in terms of the debond and pull-out lengths and other material parameters. A knowledge of these energy-absorbing processes is important since they are responsible for the toughness of the composite.

## 2. Previous work

When a composite ply fractures from an existing notch, a sequence of energy-absorbing events occurs in a region surrounding the notch tip. For example, the matrix cracks and leaves intact fibres bridging it; the fibres debond and create new surfaces. With increasing load the fibre strain energy increases, to be later dissipated when the fibres fracture some distance behind the tip of the matrix crack. The fibre then does mechanical work against frictional forces at the fibre–matrix interface when pulling free from its matrix socket (Fig. 1). These processes have been investigated and a number of models have been proposed [1–18].

The first mechanism considered was the *work of fibre pull-out*, which is due to the frictional forces that hold a broken fibre in its matrix socket. Cottrell [2] and Kelly [3] calculated the toughness of the composite due to this mechanism and their result has been widely used by others [4–14].

Outwater and Murphy [15] calculated the *debonding energy* which is the change in elastic strain energy in the fibre during fracture. The model assumes that the fibre is under a uniform stress, ignoring the frictional stress transfer between fibre and matrix. The Outwater–Murphy model has been used extensively, especially for glass-fibre reinforced thermosets, for which it was originally conceived (Kelly [4]; Harris, Beaumont and Ferran [6]; Beaumont and Phillips [7]; Fila, Bredin and Piggott [8]; FitzRandolph *et al.* [9]; Kaelble [11]; Marston *et al.* [13]).

A similar model was proposed by Piggott [16] and FitzRandolph [17], where the change in elastic strain energy of the material on fracture was equated to toughness, although only an approximate fibre stress distribution was used. The model, which is called *redistribution* or *relaxation energy*, has been used by FitzRandolph *et al.* [9] and by Marston, *et al.* [12].

Kelly [4] and Piggott [16] derived the work

*Present address: BP Research Centre, Chertsey Road, Sunbury-on-Thames, Middlesex, UK.

0022–2461/85 $03.00 + .12 

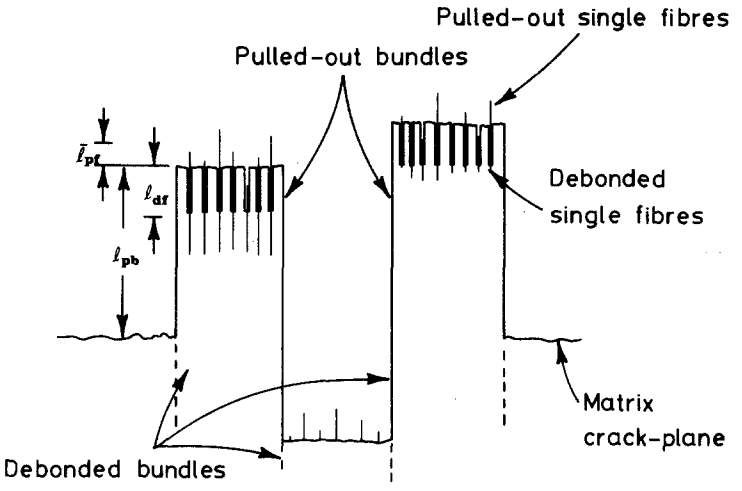


*Figure 1* Schematic diagram of a fractured composite.

done against friction after fibre debonding, but prior to fibre fracture. The dissipation of energy arises because of the different stiffness of fibre and matrix, which causes relative movement between two constituents under load. The model, known as *post-debond friction*, has been used by Harris *et al.* [18] and by Kirk *et al.* [14] to account for the toughness of glass fibres in epoxy.

The debonding, relaxation, redistribution and post-debond friction models all quantify the same energy change; their differences arise from the assumptions made and methods of derivation. A third mechanism of energy absorption, the surface energy of the fibre–matrix interface, has been discussed by Helfet and Harris [10] and by Marston *et al.* [12]. Although the surface energy of the interface is low, perhaps a few tens of Joules per square metre, the debonded area of interface can be large. This mechanism may therefore account for a substantial fraction of the total absorbed fracture energy of the composite.

In summary, several failure models for the energy-absorbing processes in composites have been proposed. Three mechanisms are identified: pull-out, surface energy, and one involving changes in the elastic strain energy of the fibre. None of the models allow for the Poisson contraction of the fibre under load, and the derivations of the elastic strain energy term by a variety of methods are all therefore approximate.

The energy absorption mechanisms may also operate on fibre bundles, and care must be taken to avoid double-counting the contributions to toughness. In general, both bundle and individual fibre debonding (and therefore pull-out) may occur in the composite. The debond length of the bundle is normally longer than that of the single fibre because of the bundle's lower debond stress and slower stress build-up [1] (Fig. 1).

This paper discusses the three principal energy-absorbing mechanisms in a single composite ply. Additional processes may operate when the plies are laminated (splitting and delamination, for instance) and have been discussed by Wells [19]).

## 3. A new analysis

### 3.1. Interfacial energy

The simplest surface energy mechanism is that due to the area of broken fibres and matrix on a plane perpendicular to the applied load, and is readily calculated using the rule of mixtures. However, this mechanism may be ignored because of the low surface energy of both fibre and matrix.

The process of debonding creates many cylindrical cracks around fibres and bundles which penetrate into the composite. Although the surface energy of the fibre–matrix interface is low, the very large surface area created by debonding leads to significant energy absorption. The energy absorption per unit area, $G^{\dagger}$, due to debonding of individual fibres of radius $r_f$ is

$$G = 2\pi r_f l_{df} 2\gamma_i \frac{V_f}{\pi r_f^2} = \frac{4 l_{df} \gamma_i V_f}{r_f} \quad (1)$$

where $l_{df}$ is the fibre debond length, $V_f$ is the fibre volume fraction, and $\gamma_i$ is the interfacial work of fracture.

For a debonded fibre bundle, a similar expression

†Throughout this work $G$ refers to the energy per unit area of crack plane, and is therefore twice the energy per unit area of crack surface, $\gamma$.

applies:

$$G = \frac{4l_{db}\gamma_b}{r_b} \quad (2)$$

where $l_{db}$ is the bundle debond length, $\gamma_b$ is the interfacial work of fracture for the bundle periphery and $r_b$ is the bundle radius. The contribution of the two components is additive, and the total toughening effect due to this mechanism is therefore

$$G_i = \frac{4l_{df}\gamma_1 V_f}{r_f} + \frac{4l_{db}\gamma_b}{r_b} \quad (3)$$

The effective surface energy for a bundle, $\gamma_b$, is given by a weighted average

$$\gamma_b = \frac{1}{a}[\pi r_f \gamma_1 + (a - 2r_f)\gamma_2]$$

where $\gamma_1$ and $\gamma_2$ are the surface energies in shear of fibre–matrix interface and pure matrix respectively, and $a$ is the centre-to-centre fibre spacing.

## 3.2. Elastic energy

After debonding, load on the fibre increases and the elastic strain energy in both fibre and matrix increases. When the fibre fractures, the energy within the debonded region is largely dissipated in the form of heat and acoustic energy. Although the stress distribution in the matrix is not known, the contribution of the matrix to toughness may be ignored because the energy density of the fibre is very much greater than that of the matrix ($E_f \gg E_m$), and the volumes of the two phases are similar.

A number of authors have calculated the change is elastic strain energy of the fibre when it debonds and snaps (Kelly [4]; Outwater and Murphy [15]; Piggott [16]; FitzRandolph [17]), but none of the analyses take detailed account of the stress distribution of the fibre. An estimation of the dissipated strain energy requires the calculation of the fibre energy before and after fracture, using the fibre stress distribution described by Wells and Beaumont [1].

### 3.2.1. Calculation of elastic energy for a single fibre

A schematic diagram of the fibre stress distribution before and after fracture is shown in Fig. 2. Remote from the matrix crack, the fibre stress is unaffected by the stress concentration around the notch and has a value $\sigma_m$. At the debond crack front the fibre stress is $\sigma_d$, rising to the failure stress in the plane of the matrix crack. After failure, the stress builds up by friction from zero at the fractured end to the mean stress level $\sigma_m$. The dissipated strain energy is therefore the difference between the initial and final states, although if failure is catastrophic then $\sigma_m$ will fall to zero.

The elastic energy stored in the debonded length of fibre, of stiffness $E_f$, just prior to fracture is

$$U_{in} = 2\int_0^{l_d/2} \pi r_f^2 \frac{[\sigma(x)]^2}{2E_f}\,dx$$

per fibre, where $\sigma(x)$ is the stress distribution in the debonded length of fibre [1], i.e.

$$\sigma(x) = \sigma_p - (\sigma_p - \sigma_d)e^{-\beta x}$$

$\sigma_p$ and $\beta$ are functions of the elastic properties of fibre and matrix ($\sigma_p$ is the maximum fibre stress due to friction, and $\sigma_d$ is the fibre debond stress). For simplicity let

$$A = \sigma_p - \sigma_d \text{ and } X = \frac{l_d}{2}$$

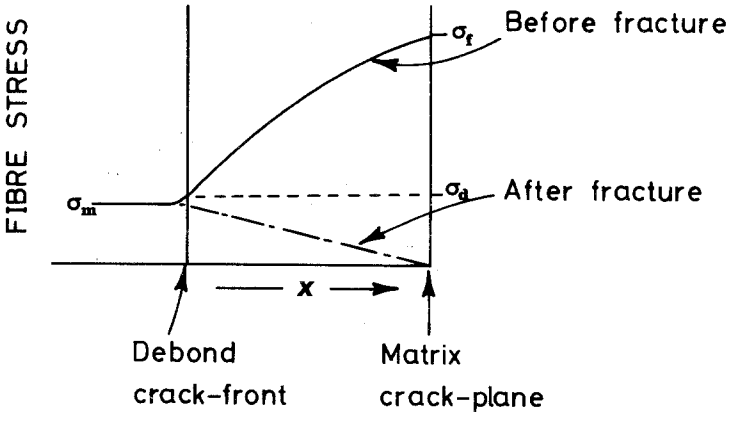


*Figure 2* Schematic diagram of fibre stress distribution before and after fracture.

Then

$$U_{in} = \frac{\pi r_f^2}{E_f}\left|\sigma_p^2 X - \frac{A^2(e^{-2\beta x}-1)}{2\beta} + \frac{2\sigma_p A(e^{-\beta X}-1)}{\beta}\right| \quad (4)$$

The energy stored in the fibre after fracture may be estimated to sufficient accuracy by assuming a linear stress distribution as shown in Fig. 2, i.e.

$$\sigma(x) = \sigma_m\left(1-\frac{x}{X}\right)$$

and the energy per fibre is therefore

$$U_{out} = \frac{\pi r_f^2}{E_f}\int_0^X [\sigma(x)]^2\,dx = \frac{\pi r_f^2}{E_f}\left|\frac{\sigma_m^2 X}{3}\right| \quad (5)$$

Taking the difference between Equations 5 and 4, the toughening due to the absorbed elastic energy when a debonded fibre snaps is

$$G_{el} = \frac{V_f}{E_f}\left|\frac{\sigma_p^2 l_d}{2} - \frac{(\sigma_p-\sigma_d)^2(e^{-\beta l_d}-1)}{2\beta} + \frac{2\sigma_p(\sigma_p-\sigma_d)(e^{-\beta l_d/2}-1)}{\beta} - \frac{\sigma_m^2 l_d}{6}\right| \quad (6)$$

The mean stress level $\sigma_m$ is taken as zero in this work.

### 3.2.2. Calculation of elastic energy for fibre bundles

The process of bundle debonding has been discussed by Wells and Beaumont [1] where the bundle is treated as a large fibre having the elastic properties of the composite ply. Similarly, the dissipation of elastic energy due to bundle fracture may be calculated using Equation 6, after substitution of the appropriate material properties. The elastic energy absorption of the composite ply may be estimated by the term for the bundle only, since this inherently takes account of the single fibre energy changes.

## 3.3. Work of pull-out

Cottrell [2] and Kelly [3] first calculated the work done against frictional forces when pulling a fibre from its matrix socket. Their derivation may be amended to take account of the Poisson contraction of the fibre during pull-out.

### 3.3.1. Pull-out work for a single fibre

The pull-out stress for a fibre embedded a distance $x$ is, from [1],

$$\sigma(x) = \sigma_p(1-e^{-\beta x})$$

and the work to pull out a single fibre a distance $l$ is therefore

$$W = \int_0^l \pi r_f^2 \sigma(x)\,dx$$

The fracture energy per unit area is

$$G_p(l) = V_f\sigma_p\left|l + \frac{(e^{-\beta l}-1)}{\beta}\right| \quad (7)$$

If the average pull-out length is $\bar{l}_p$ then, to a good approximation, the average energy absorption due to pull-out is

$$\bar{G}_p = V_f\sigma_p\left|\bar{l}_p + \left(\frac{e^{-\beta\bar{l}_p}-1}{\beta}\right)\right| \quad (8)$$

### 3.3.2. Pull-out work for a fibre bundle

The energy absorption due to the phenomenon of bundle pull-out may be estimated from Equation 8, after substitution of the appropriate bundle properties. The pull-out energies due to fibre and bundle pull-out are additive.

## 4. Theoretical toughness and toughness mapping

The energy absorption due to the fracture of a composite ply is due essentially to three principal failure mechanisms. The failure models are functions of material properties, such as fibre modulus and strength, as well as the debond and pull-out lengths of individual fibres and bundles of fibres. These characteristic lengths can in turn be calculated from the material properties [1]. By combining these results, the composite toughness may now be calculated directly from the properties of the fibre, matrix and interface.

One effect of combining, for example, a theory of pull-out with that of energy absorption is to highlight the complex interdependencies that exist in the system. By way of example, consider the result of reducing the frictional stress between fibre and matrix. This increases the pull-out length, but also reduces the work done in pulling the fibre out of its socket. The overall effect on toughness is therefore not obvious. The models described above are not restricted to a particular fibre system. Their results may therefore be used for glass, Kevlar, and high-modulus and high-

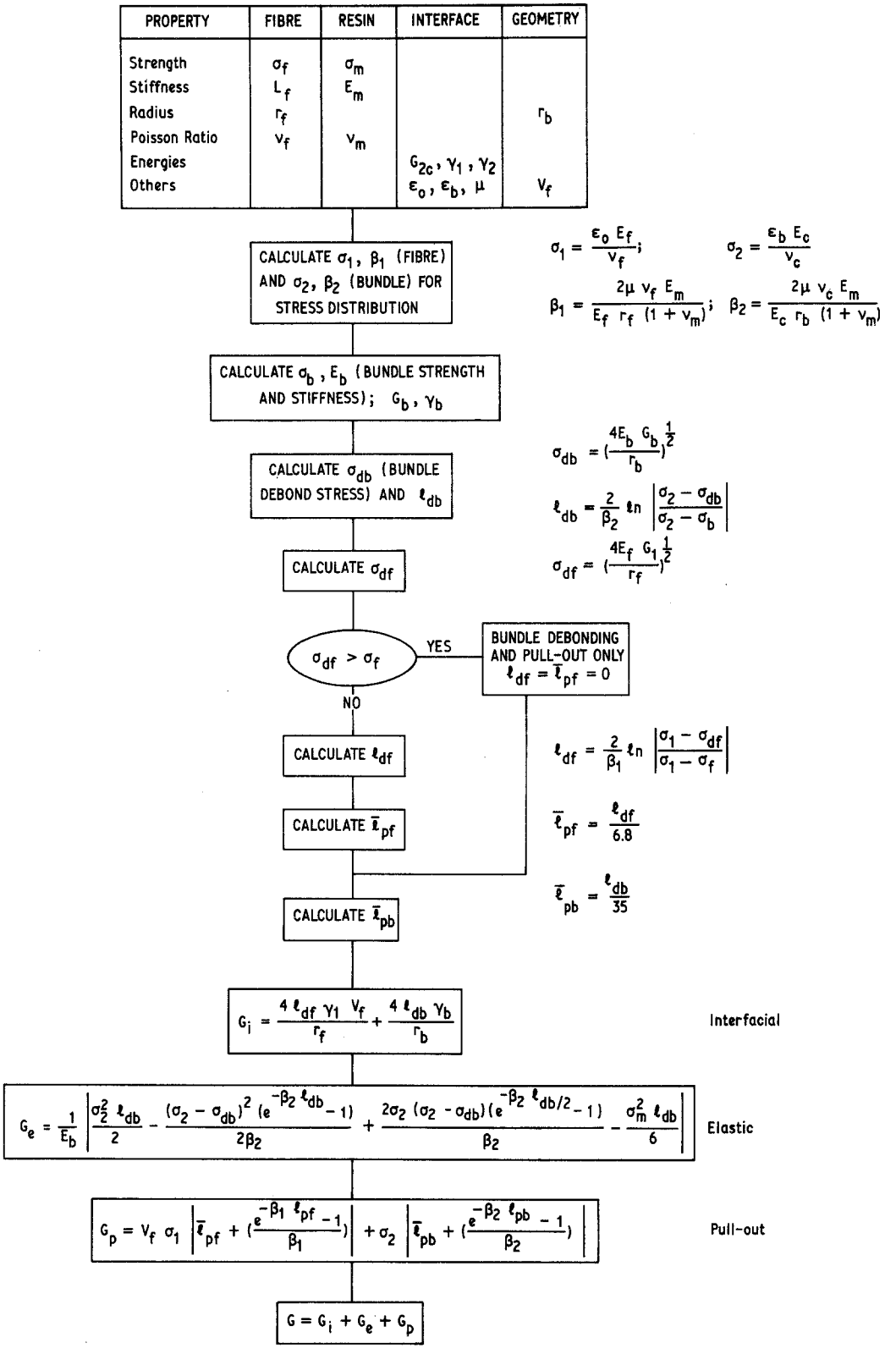


*Figure 3* Method of calculating composite toughness.

TABLE I Fibre properties used in calculations

| Fibre property | E-glass | Kevlar | High-modulus carbon | High-strength carbon |
|---|---|---|---|---|
| Average fibre strength $\sigma_f$ (GPa) | 1.65 | 2.27 | 1.79 | 2.48 |
| Fibre Young's modulus $E_f$ (GPa) | 70 | 124 | 370 | 230 |
| Fibre radius $r_f$ ($\mu$m) | 7 | 6 | 4 | 4 |
| Weibull modulus $m$ | 7 | 7 | 7 | 7 |
| Interfacial toughness $G_1$ (J m$^{-2}$) | 50 | 2 | 24 | 61 |
| Fibre Poisson's ratio $\nu_f$ | 0.2 | 0.2 | 0.2 | 0.2 |

strength carbon fibres, after substitution of the appropriate material properties.

## 4.1. Method of calculation

A prediction of composite toughness based on Equations 3, 6 and 8 requires the prior calculation of debond length and pull-out length for both individual fibres and fibre bundles [1]. In addition, the frictional stress distribution parameters $\sigma_p$ and $\beta$ have to be determined from the elastic properties of the materials [1]. Fig. 3 shows the order of calculation and the relevant equations.

## 4.2. Estimation of the input parameters for the model

The model requires fifteen parameters in all; many of these are well known and can be found from the literature (e.g. stiffness and strength of fibre and matrix). Values of the parameters used for E-glass, Kevlar 49, and high-modulus and high-strength carbon fibres are given in Tables I to III. The justification for the choice of values of those parameters which are not easily measured is provided below.

### *4.2.1. Interfacial work of fracture*

The work of fracture for shear failure of the fibre–matrix interface, $G_1$, and the pure matrix, $G_2$, have been estimated from tests on single bundles of glass fibres in epoxy resin. Values of $G_1 = 50\,\mathrm{J\,m^{-2}}$ and $G_2 = 500\,\mathrm{J\,m^{-2}}$ were measured [19]. These values, in conjunction with the inter-laminar shear strengths, may be used to estimate the value of $G_1$ for different fibre systems [19]. The approximate values found are given in Table IV. The values of $G_1$ and $G_2$ are used to estimate the energy absorption due to the creation of new interface (Equation 3), since $G_1 = 2\gamma_1$ and $G_2 = 2\gamma_2$.

TABLE II Epoxy matrix properties used in calculations

| | |
|---|---|
| Matrix strength $\sigma_m$ (MPa) | 80 |
| Matrix Young's modulus $E_m$ (GPa) | 3 |
| Shear toughness $G_2$ (J m$^{-2}$) | 500 |
| Poisson's Ratio $\nu_m$ | 0.35 |

### *4.2.2. Fibre–matrix misfit strain ($\epsilon_0$)*

A number of authors have investigated the residual stresses around fibres produced by the mismatch between thermal coefficients of expansion of fibre and matrix [20–26]. A summary of results is shown in Table V. An estimate of the effective radial compressive stress obtained by Adams [23] for glass fibres in epoxy is 8.7 MPa. A typical radial compressive stress of 3 MPa is predicted by Woolstencroft and Curtis [24]. Cunningham *et al.* [25] measured a radial compressive stress of 6 MPa for a $ZrO_2$ glass fibre in epoxy. Harris [26] calculated a misfit strain of about 0.8%, from which a radial stress can be obtained by using a shrink-fit equation derived by Timoshenko [27]. A value of $\epsilon_0 = 0.65\%$ has been used in this work. The value is similar to those predicted, although higher than most of the finit-element estimates. The same value is used for all fibre systems, as there is little evidence that the misfit strain is strongly affected by fibre type.

### *4.2.3. Bundle misfit strain*

Experiments carried out on single glass fibre bundles in epoxy indicate a bundle misfit strain of about 5% [19]. If it is assumed that the bundle misfit is due to a fixed number of intermeshed fibres across the bundle diameter, then the misfit strain will be proportional to the fibre radius and bundle radius (Section 4.2.5.). A value of $\epsilon_b = 5\%$ has been used for E-glass, which is in agreement with the experimental estimate; values for these and other fibres are given in Table VI.

### *4.2.4. Coefficient of friction*

The coefficient of friction between glass and epoxy was found by simple experiment. A piece of polished epoxy was placed on a sheet of plate glass

TABLE III Other parameters used in toughness maps

| Composite property | E-glass | Kevlar | High-modulus carbon | High-strength carbon |
|---|---|---|---|---|
| Coefficient of friction $\mu$ | 0.25 | 0.25 | 0.25 | 0.25 |
| Poisson's ratio $\nu_c$ | 0.32 | 0.32 | 0.32 | 0.32 |
| Bundle radius $r_b$ ($\mu$m) | 200 | 200 | 200 | 200 |
| Bundle misfit strain $\epsilon_b$ (%) | 5 | 4.3 | 2.9 | 2.9 |
| Fibre misfit strain $\epsilon_0$ (%) | 0.65 | 0.65 | 0.65 | 0.65 |
| Volume fraction $V_f$ (%) | 60 | 60 | 60 | 60 |

TABLE IV Interface shear toughness of composites

| Fibre type | $G_i$ (J m$^{-2}$) |
|---|---|
| High-modulus carbon | 24* |
| High-strength carbon | 61* |
| Kevlar 49 | 2* |
| E-glass | 50† |

*Calculated; †measured.

after both items had been degreased. The plate was tilted until sliding just occurred. A repeatable value for the coefficient of friction, $\mu = 0.25$, was found. The same value is used for all fibres, since any error in the value of $\mu$ is likely to be small by comparison with the error in $\epsilon_0$ and $\epsilon_b$, with which it always appears.

### 4.2.5. Bundle radius

The bundle radius is a difficult parameter to estimate. Observations of failed laminates suggest that the bundles are about 0.5 mm wide and with a thickness equal to that of the composite ply. This correponds to an effective bundle radius of about 200 $\mu$m, which is the value used in the model.

### 4.2.6. Fibre volume fraction

The model assumes a volume fraction of 60%, a value typical of high-quality laminates.

## 4.3. Construction of fracture energy maps

The mechanisms which control the toughness of a

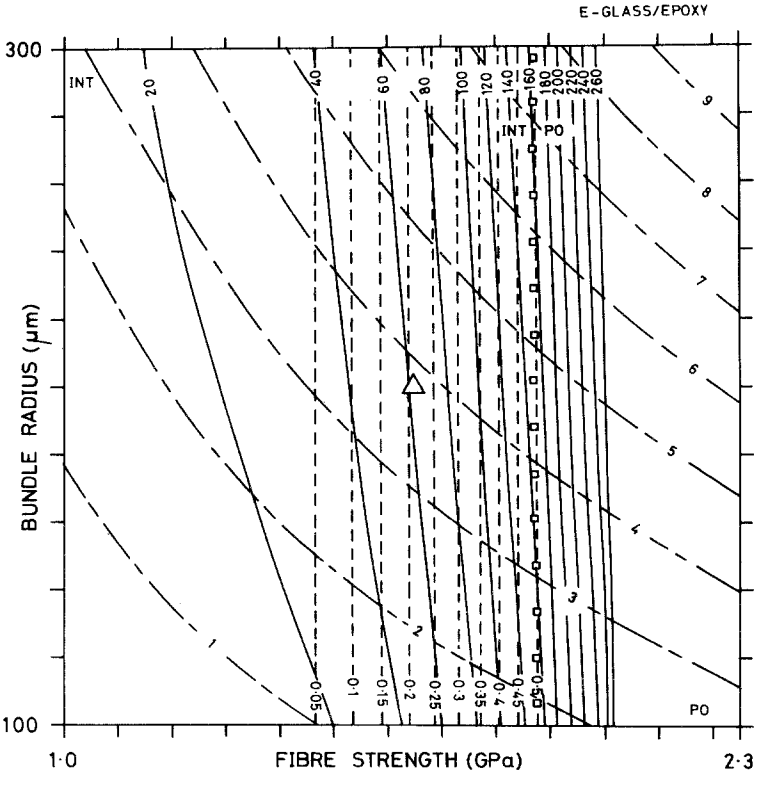


*Figure 4* A typical fracture map, showing the effect of varying bundle radius and fibre strength on the toughness of E-glass/epoxy.

TABLE V Estimates of misfit strain

| Authors | Radial stress (MPa) | misfit strain (%) | Notes |
|---|---|---|---|
| Adams [23] | 8.7 | 0.4 | $V_f = 60\%$, S-glass fibre |
| Woolstencroft and Curtis [24] | 3.45 | 0.18 | $V_f = 40\%$, carbon fibre |
| | 3.21 | 0.16 | $V_f = 65\%$, carbon fibre |
| | 16.2 | 0.82 | $V_f = 80\%$, carbon fibre |
| | 22.8 | 1.2 | $V_f = 89\%$, carbon fibre |
| Cunningham, Sargent and Ashbee [25] | 6 | 0.28 | Model, glass fibre |
| Harris [26] | – | 0.8 | Any fibre, little affected by volume fraction |

TABLE VI Bundle misfit strains

| | $r_f$ ($\mu$m) | $\epsilon_b$ (%) |
|---|---|---|
| E-glass | 7 | 5 |
| Kevlar 49 | 6 | 4.3 |
| Carbon | 4 | 2.9 |

composite ply have been shown to interact in a complex way, making it difficult to predict the effect of changing material properties on toughness. A "mapping" technique used in this work enables the effect of two simultaneously varying parameters upon toughness to be shown clearly. A typical map for E-glass/epoxy is shown in Fig. 4.

### 4.3.1. Method of computation

A computer program has been written to produce the map; it allows any of the variables which affect the fracture process to be varied along the $x$ and $y$ axes. To construct a map the values of the $x$ and $y$ parameters are varied in sequence, all other material properties are held at the default values listed in Tables I to III. The pull-out and debond lengths for fibres and bundles are calculated at each point, and the composite toughness found as described in Section 4.1. Contours of the fibre and bundle pull-out lengths, the bundle debond length, and the composite toughness are then found by

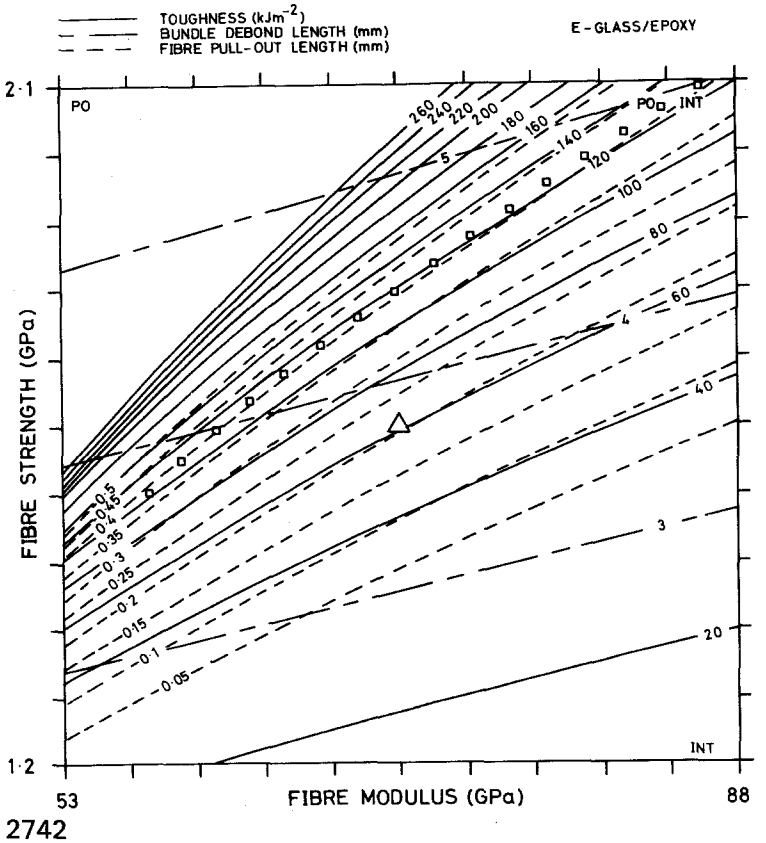


*Figure 5* E-glass/epoxy fracture map with axes of fibre strength and fibre modulus.

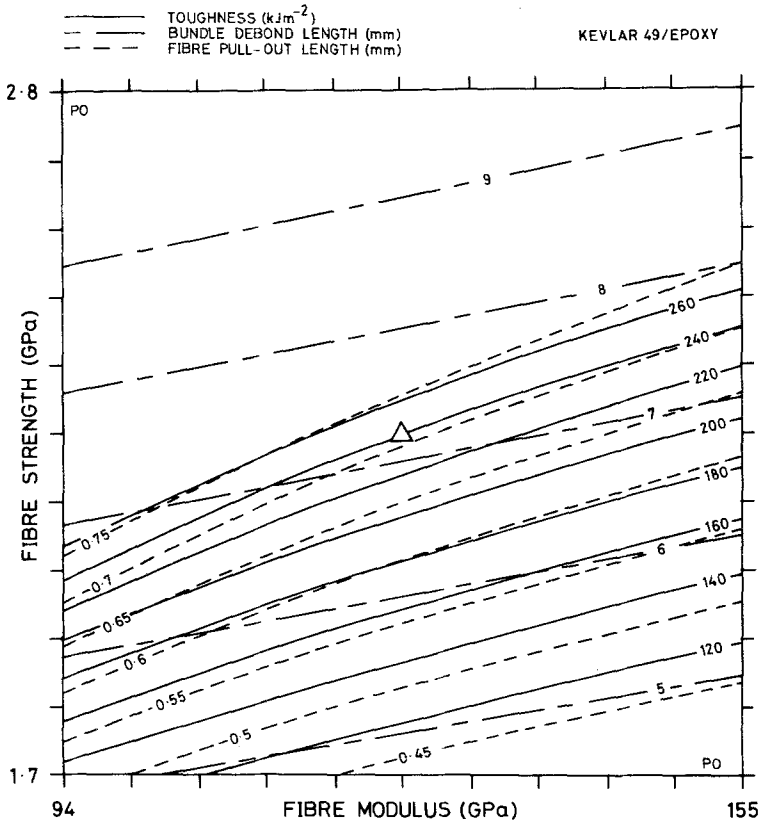


*Figure 6* Kevlar/epoxy fracture map with axes of fibre strength and fibre modulus.

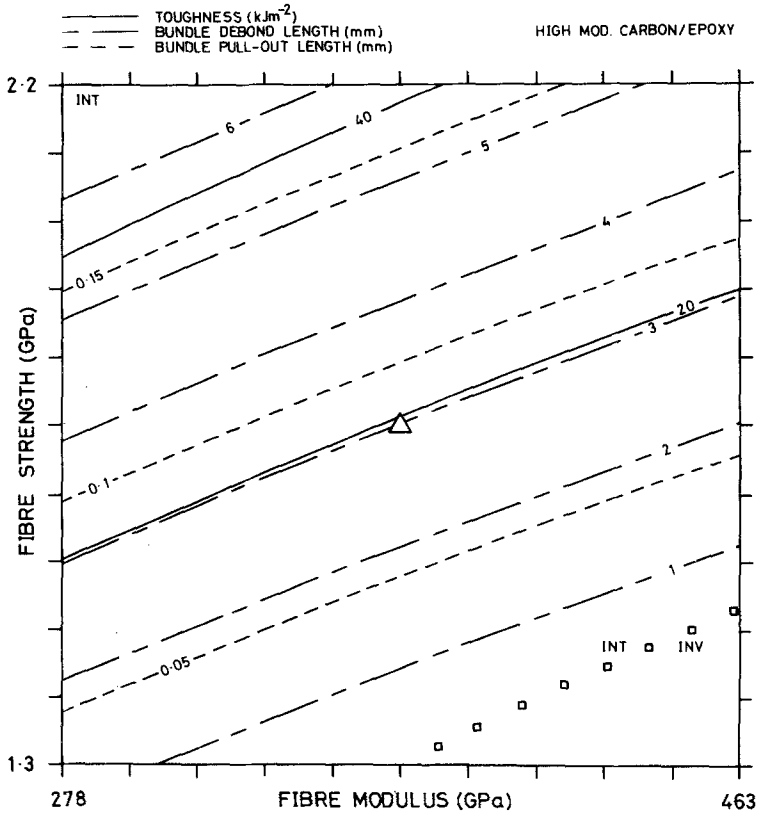


*Figure 7* High-modulus carbon/epoxy fracture map with axes of fibre strength and fibre modulus.

TABLE VII Contour values used in computation

| Parameter | Contour value | | |
|---|---|---|---|
| | Lowest | Highest | Increment |
| Fibre pull-out length $\bar{l}_{pf}$ (mm) | 0.05 | 0.5* | 0.05 |
| Bundle pull-out length $\bar{l}_{pb}$ (mm) | 0.05 | 0.5 | 0.05 |
| Bundle debond length $\bar{l}_{db}$ (mm) | 1 | 10 | 1 |
| Toughness $G$ (kJ m$^{-2}$) | 20 | 260 | 20 |

*Contours extend to $\bar{l}_{pf}$ = 0.75 mm on Kevlar maps

linear interpolation from the actual points of calculation.

### 4.3.2. Description of a typical map

Fig. 4 shows a map produced for E-glass/epoxy, using the values listed in the Tables. The contours are identified by the differing hatch lengths, and are labelled as detailed in Table VII. The largest single toughening mechanism (the "dominant mechanism") is identified at each calculation point; the boundary between areas with different dominant mechanisms is shown by a series of small squares. The regions are identified by the abbreviations

PO = Pull-out energy

EL = Elastic energy

INT = Interfacial energy

which are printed on either side of the boundary. In addition, the label INV indicates a region where debond length theory is invalid.

## 4.4. Comparison of fracture maps for different systems

Maps have been produced for glass, Kevlar, high-modulus and high-strength carbon-fibre composites. Figs. 5 to 8 show four such maps. All have fibre strength and fibre modulus as axes, varying from 75% to 125% of the nominal values for the fibre. The maps all show toughness increasing rapidly with fibre strength, and decreasing slowly

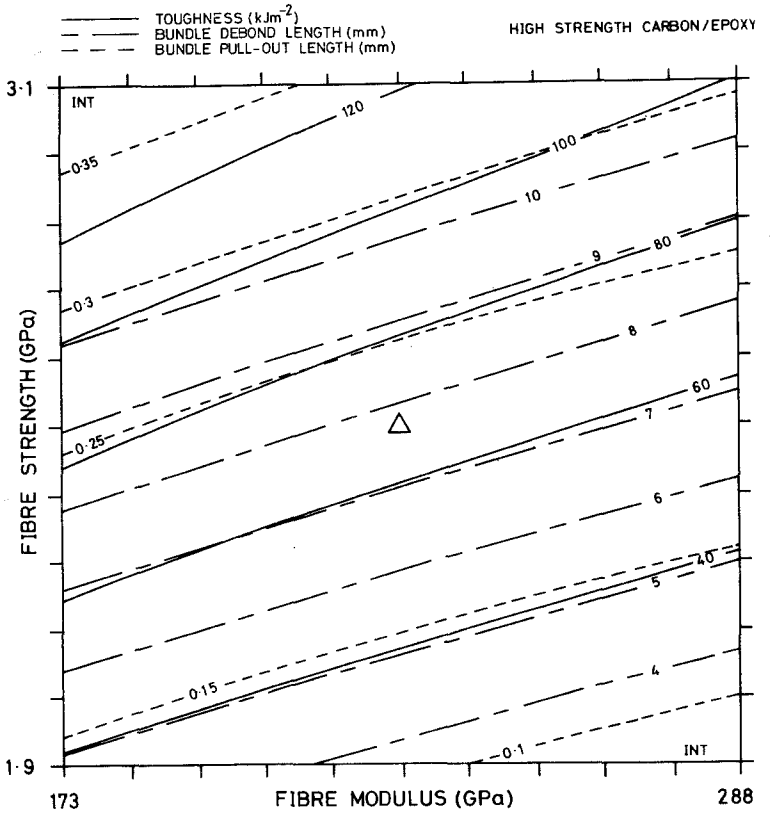


*Figure 8* High-strength carbon/epoxy fracture map with axes of fibre strength and fibre modulus.

TABLE VIII Predicted properties of composites*

| Fibre type | Pull-out length | | Bundle debond length $l_{db}$ (mm) | Toughness $G$ (kJ m$^{-2}$) | Dominant mechanism |
|---|---|---|---|---|---|
| | Fibre $\bar{l}_{pf}$ (mm) | Bundle $\bar{l}_{pb}$ (mm) | | | |
| Glass | 0.21 | (~ 0.1) | 3.8 | 61 | Interface |
| Kevlar | 0.71 | (~ 0.3) | 7.2 | 240 | Pull-out |
| High modulus carbon | (0) | 0.09 | 2.9 | 19 | Interface |
| High-strength carbon | (0) | 0.22 | 7.7 | 67 | Interface |

*Figures in brackets are not contoured on the maps.

with increasing fibre stiffness. The predictions for the "typical" material (marked by the triangle) are summarized in Table VIII. The values of material properties used in the calculations of these maps have been taken directly from the results of Section 4.2 and the Tables.

The main points of interest are that the model predicts reasonable estimates of both lengths and toughnesses for all the systems, despite the variation in fibre properties. In particular, the model predicts pull-out to be entirely of bundles in carbon composites, and principally of individual fibres ($l_{pf} > l_{pb}$) in glass and Kevlar; this is observed in practice. The predicted toughness of Kevlar is high, in agreement with its known high impact performance. This contrasts with the poor impact behaviour of high-modulus carbon composites, which is also predicted*. The toughenss of Kevlar is largely due to pull-out energy, which is only fully developed when the matrix crack faces are well separated. Consequently the toughness found from notched strength tests, where the crack opening is limited, will be lower than the value shown on the map.

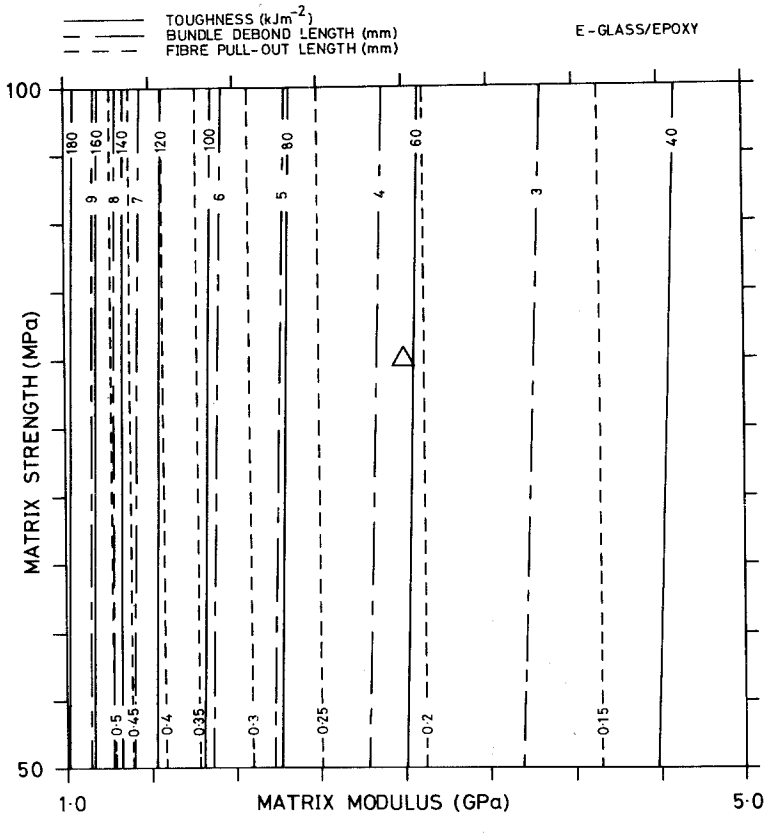


*Figure 9* E-glass/epoxy fracture map with axes of matrix strength and matrix modulus.

*The details of energy absorption may differ at high strain rates, but the values predicted here are thought to indicate relative impact properties.

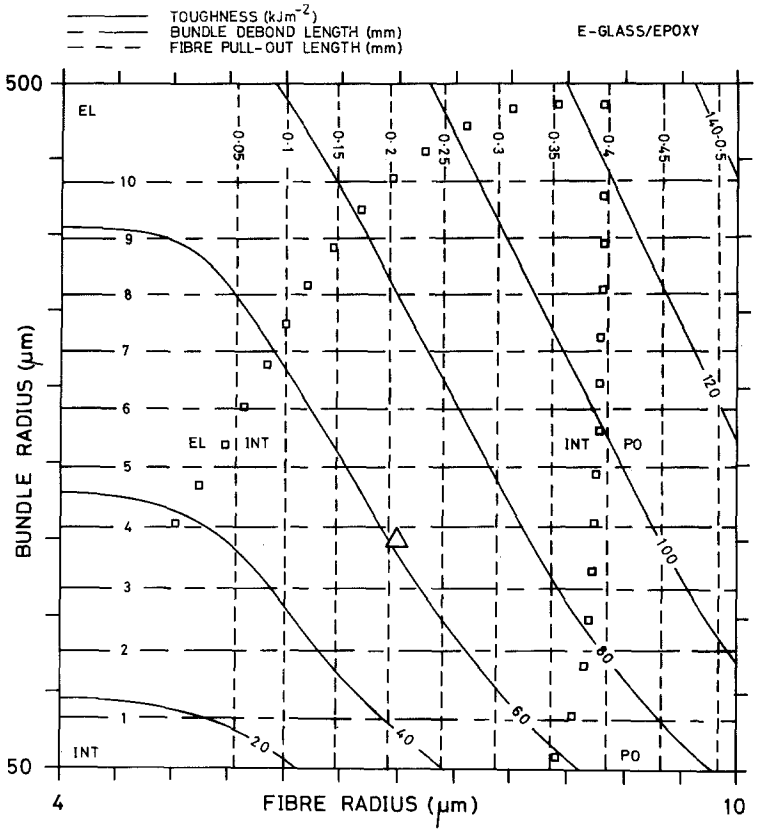


*Figure 10* E-glass/epoxy fracture map with axes of bundle radius and fibre radius.

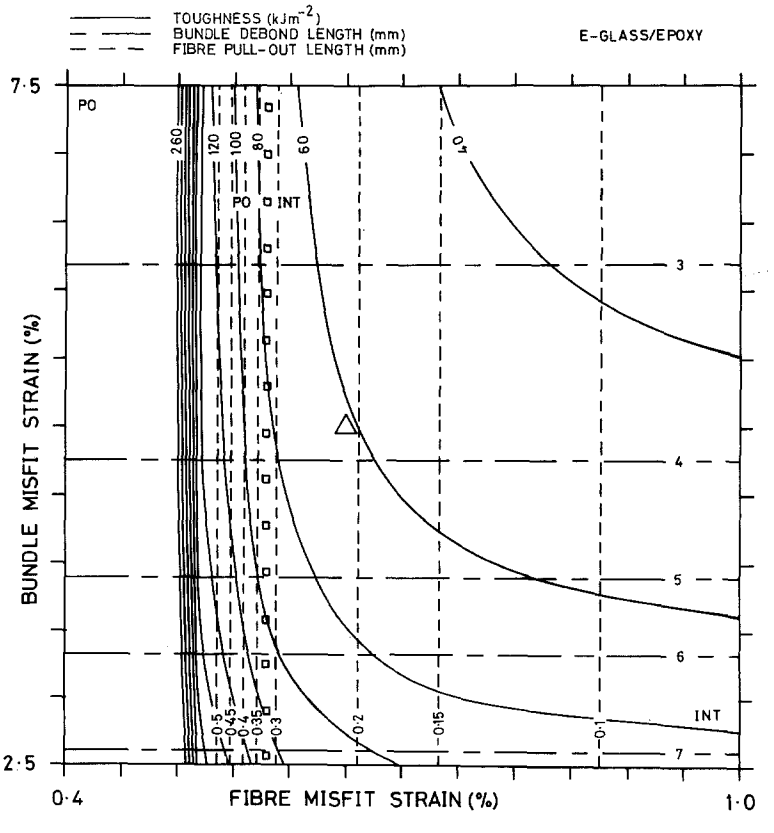


*Figure 11* E-glass/epoxy fracture map with axes of bundle misfit strain and fibre misfit strain.

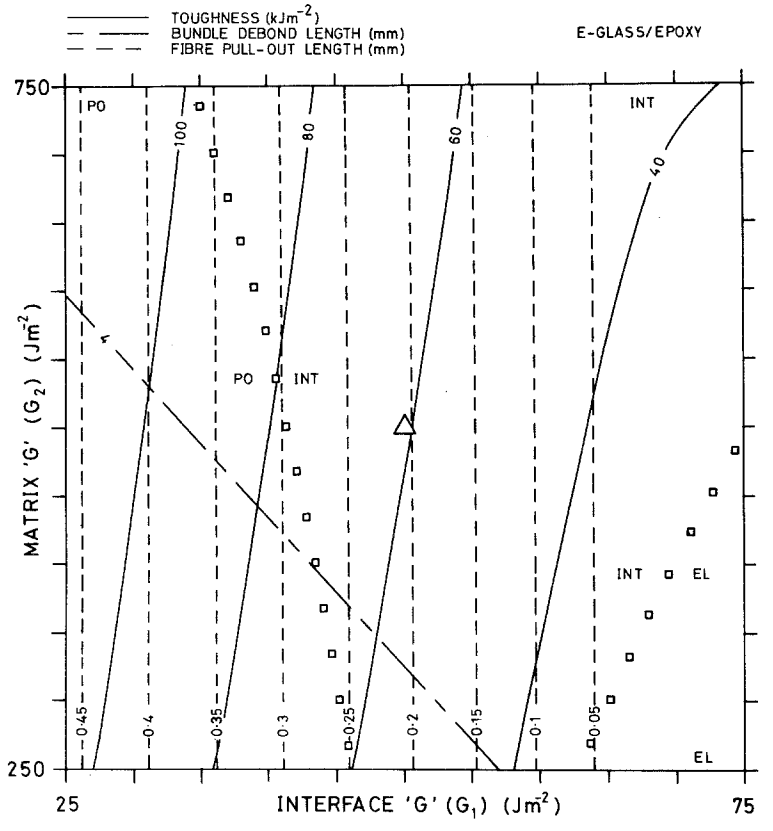


*Figure 12* E-glass/epoxy fracture map with axes of matrix toughness and interface toughness.

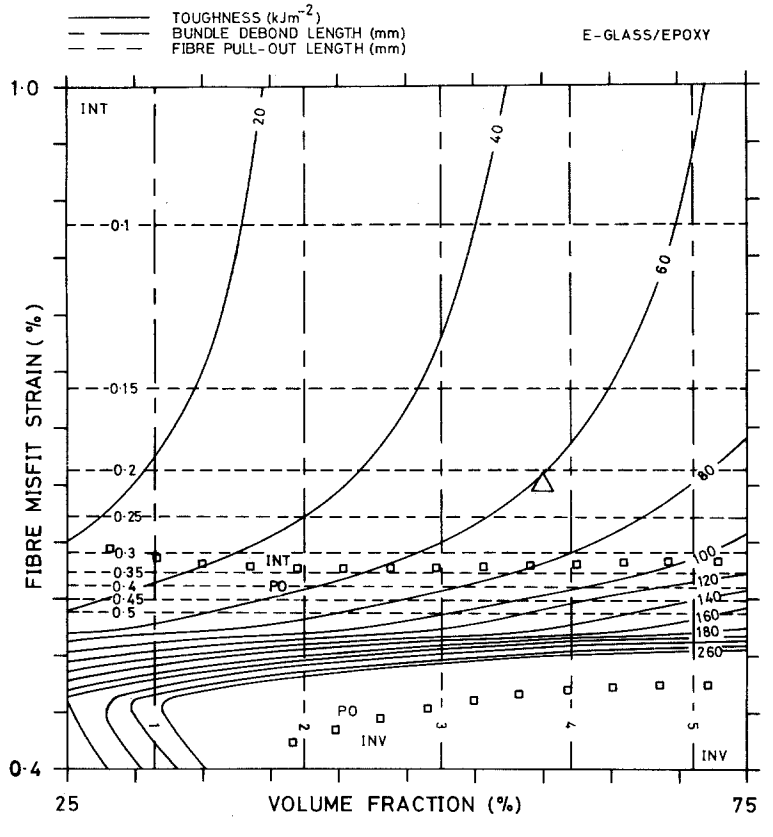


*Figure 13* E-glass/epoxy fracture map with fibre misfit strain and volume fraction.

TABLE IX Summary of fracture property dependence on constitutive properties of the composite*

| Composite Parameter | Glass and Kevlar fibre composites | | | | Carbon fibre composites | | |
|---|---|---|---|---|---|---|---|
| | Effect on | | | Notes | Effect on | | |
| | $l_{pf}$ | $l_{db}$ | $G$ | | $l_{pb}$ | $l_{db}$ | $G$ |
| $\sigma_f$ | ↑ | ↑ | ↑ | Direct effect of $l_p$ and $l_d$ | ↑ | ↑ | ↑ |
| $E_f$ | ↓ | ↓ | ↓ | Increases debond stress | ↓ | ↓ | ↓ |
| $\sigma_m$ | – | – | – | Negligible effect on strength of bundle | – | – | – |
| $E_m$ | ↓ | ↓ | ↓ | Residual stress for a given misfit strain affected | ↓ | ↓ | ↓ |
| $r_f$ | ↑ | – | ↑ | Fibre debond stress and friction build-up affected | – | – | – |
| $r_b$ | – | ↑ | ↑ | Reduced bundle debond stress and friction build-up | ↑ | ↑ | ↑ |
| $\epsilon_0$ | ↓ | – | ↓ | Faster friction stress build-up | – | – | – |
| $\epsilon_b$ | – | ↓ | ↓ | Faster friction stress build-up | ↓ | ↓ | ↓ |
| $G_1$ | ↓ | ↓ | ↓ | Debond stress and interface energy | ↓ | ↓ | ↓ |
| $G_2$ | – | ↓ | ↓ | Debond stress and interface energy | ↓ | ↓ | ↑ |
| $V_f$ | – | ↑ | ↑ | Increased number of fibres, increased bundle strength | ↑ | ↑ | ↑ |

*↑, increases with composite parameter; ↓, decreases.

### 4.5. Parametric study of fracture parameters

The toughness models are dependent on fifteen parameters. The effect of some may be small, and some may be assumed constant for practial purposes (e.g. $\mu$, $\nu_f$, $\nu_m$ and $m$). The parameters are from four categories:

| | |
|---|---|
| Fibre | $\sigma_f, E_f, r_f, m, \nu_f$ |
| Matrix | $\sigma_m, E_m, G_1, \nu_m$ |
| Interface | $\mu, \epsilon_0, \epsilon_b, G_1$ |
| Geometry | $r_b, V_f$ |

The effect of changes in the Weibull modulus of the fibre, $m$, has not been discussed in this paper although its effect on pull-out lengths was described by Wells [19]. The influence of other variables on pull-out lengths, debond lengths and composite toughness is displayed on fracture maps. Maps for E-glass/epoxy (Figs. 9 to 13) show a small triangle marking the location of the "typical" composite. The results are summarized in Table IX; Kevlar and E-glass composites have the same dependence on material properties. The behaviour of carbon composites is also shown in Table IX.

## 5. Summary and conclusions

1. Three mechanisms of energy absorption are proposed, and are used in conjunction with previously developed theories of pull-out and debonding.

2. The toughness of composite laminae is predicted from fibre, matrix and interface properties, and the results displayed in the form of "toughness maps".

3. A parametric study indicates the key material variables which control toughness, allowing the prospect of obtaining higher toughness by increasing fibre strength, fibre radius, tow size, and volume fraction; or by reducing fibre or matrix stiffness, fibre–matrix bond strength, and fibre–matrix misfit strains induced on cure. Although changes in many of these parameters will affect other properties of the composite this paper quantifies their effect on toughness, enabling better optimization of material performance.

## Acknowledgements

The authors wish to acknowledge helpful discussions with Professor M. F. Ashby. One of us (JKW) acknowledges the support of the Science and Engineering Research Council in the form of a Research Studentship during the course of this work.

## References

1. J. K. WELLS and P. W. R. BEAUMONT, *J. Mater. Sci.* **20** (1985) 1275.
2. A. H. COTTRELL, *Proc. Roy. Soc.* **A282** (1964) 2.
3. A. KELLY, *ibid.* **A282** (1964) 63.
4. *Idem, ibid.* **A319** (1970) 95.
5. J. G. MORLEY, *ibid.* **A319** (1970) 117.
6. B. HARRIS, P. W. R. BEAUMONT and E. DE FERRAN, *J. Mater. Sci.* **6** (1971) 238.
7. P. W. R. BEAUMONT and D. C. PHILLIPS, *ibid.* **7** (1972) 682.
8. M. FILA, C. BREDIN and M. R. PIGGOTT, *ibid.* **7** (1972) 983.

9. J. FITZRANDOLPH, D. C. PHILLIPS, P. W. R. BEAUMONT and A. S. TETELMAN, *ibid.* 7 (1972) 289.
10. J. L. HELFET and B. HARRIS, *ibid.* 7 (1972) 494.
11. D. H. KAELBLE, *J. Adhesion* 5 (1973) 245.
12. T. H. MARSTON, A. G. ATKINS and D. K. FELBECK, *J. Mater. Sci.* 9 (1974) 447.
13. M. R. PIGGOTT, *ibid.* 9 (1974) 494.
14. J. N. KIRK, M. MUNRO and P. W. R. BEAUMONT, *ibid.* 13 (1978) 2197.
15. J. D. OUTWATER and M. C. MURPHY, Paper 11c, 24th Annual Technical Conference on Composites Section, SPI (1969).
16. M. R. PIGGOTT, *J. Mater. Sci.* 5 (1970) 669.
17. J. FITZRANDOLPH, MS thesis, University of California, Los Angeles, 1971.
18. B. HARRIS, J. MORLEY and D. C. PHILLIPS, *J. Mater. Sci.* 10 (1975), 2050.
19. J. K. WELLS, PhD thesis, University of Cambridge, 1982.
20. J. K. WELLS and P. W. R. BEAUMONT, *J. Mater. Sci.* 17 (1982) 397.
21. D. F. ADAMS and A. K. MILLER, *J. Compos. Mater.* 11 (1977) 285.
22. A. K. MILLER and D. F. ADAMS, ASTM STP 658 (American Society for Testing and Materials Philadelphia, 1978) p. 121.
23. D. F. ADAMS, Proceedings of the 24th National SAMPE Symposium and Exhibition, San Francisco, 1979.
24. D. H. WOOLSTENCROFT and A. R. CURTIS, PRI Conference on "Interfaces in Composites", University of Liverpool, April 1981.
25. B. CUNNINGHAM, J. P. SARGENT and K. H. G. ASHBEE, *J. Mater. Sci.* 16 (1981) 620.
26. B. HARRIS, *ibid.* 13 (1978) 173.
27. S. TIMOSHENKO, "Strength of Materials", Part II, 2nd edn. (MacMillan, London, 1941 p. 24.

*Received 28 June*
*and accepted 10 July 1984*